Flow evolution and vertical accelerations in wave-swash interactions

Claudio Meza–Valle[1], Nimish Pujara[1]

[1]Department of Civil and Environmental Engineering, University of Wisconsin-Madison, Madison, Wisconsin 53706, USA

Key Points:

- Wave-swash interactions can be characterized by the ratio of consecutive wave heights and the dimensionless time separation between them.
- Large upward-directed vertical accelerations that often exceed gravity are observed for certain wave-swash interactions.
- During large upward-directed vertical accelerations, the flow velocity is upward- and onshore-directed.

Corresponding author: Claudio Meza–Valle, `meza4@wisc.edu`

Abstract

We report on a laboratory study of wave-swash interactions, which occur in the very nearshore environment of a beach when the shallow swash flow of a breaking wave interacts with a subsequent wave. Wave-swash interactions have been observed in the field, hypothesized to be important for nearshore transport processes, and categorized into different qualitative types, but quantitative descriptions of their dynamics have remained elusive. Using consecutive solitary waves with different wave heights and separations, we are able to reliably and repeatably generate a wide variety of wave-swash interactions with large flow velocities and vertical accelerations. We find that wave-swash interactions can be quantitatively characterized in terms of two dimensionless parameters: H_2/H_1 and $T_{\text{sep}}/T_{\text{swash}}$, where the first is the wave height ratio for consecutive waves and the second is a dimensionless measure of the time separation between consecutive wave crests. We find that wave-swash interactions commonly involve three main stages and that the cross-shore location of these stages is dependent on the interaction type. Using measurements of bed pressure and free-surface displacement, we estimate the total vertical accelerations and focus on the peak upward-directed acceleration. We find that wave-swash interactions can generate vertical accelerations that can easily exceed gravity, despite occurring in very shallow water depths. The vertical velocities during large vertical accelerations are upward-directed and are quickly followed by onshore-directed horizontal velocities. Together, our findings suggest that wave-swash interactions are capable of inducing large material suspension events of sediment or solutes in sediment pores, and transporting them onshore.

Plain Language Summary

Waves arriving at a beach create fast shallow flows that are responsible for moving large amounts of sediment. Here, we consider how the flow due to one wave interacts with the next wave to arrive in idealized wave tank experiments. We find that in such interactions, flows moving in opposite directions can collide and create large, but short-lived peaks in upward-directed flow and acceleration. These peaks in flow and acceleration are likely to drive movement of material such as sediment and dissolved constituents in ways that are currently not taken into account. We also hypothesize that the vertical accelerations are sufficiently strong to destabilize a sediment bed.

1 Introduction

Water waves continuously shape sandy coastlines through sediment transport across a wide range of timescales, from sediment suspension events caused by individual waves to beach morphology changes that occur over seasons or longer [e.g., Mart´inez et al. (2018); Toimil et al. (2020)]. Hydrodynamically, waves transformation near the coast is classified into several sub-regions such as the surf zone and swash zone (Dean & Dalrymple, 2004; Holthuijsen, 2007; Jackson & Short, 2020). In the swash zone, flow begins with the shoreward acceleration of the shoreline with the arrival and collapse of each wave, and is characterised by the movement of water up and down the beach, delimited by a cycle of upwash and backwash, otherwise referred to as a swash event (Brocchini & Baldock, 2008). In particular, wave-swash interactions are events where incoming waves collide with the upwash or backwash flows of the previous swash event. Wave-swash interactions have been qualitatively described in the field [e.g., Hughes and Moseley (2007); Erikson et al. (2005)] and hypothesized to be an important mechanism for sediment transport [e.g., Puleo et al. (2000); Elfrink and Baldock (2002); Puleo and Butt (2006); Alsina et al. (2009); Puleo and Torres-Freyermuth (2016)] for some time.

The qualitative descriptions and types of wave-swash interactions include: (a) Wave-upwash interactions, where the upwash flow of a wave catches the upwash flow of the previous wave; (b) Weak wave-backwash interactions, where the upwash flow of a wave catches

with the backwash flow of the previous wave, with the result that the flow is again pushed shoreward; and (c) Strong wave-backwash interactions, which are physically similar to weak wave-backwash interactions, but with result that the interaction induces a stop or receding of the incoming flow, often accompanied by a stationary hydraulic jump. In many field scenarios, the development of 'free swash events' (no interactions) tend to occur on the upper beach, whereas wave-swash interactions are common in the lower beach. For an incident wave train with constant wave heights, the time between wave crests relative to the timescale of the swash event has been used to understand these interactions (Baldock & Holmes, 1999; Lo et al., 2013; Pujara et al., 2015a), but this has been insufficient to understand the broad class of wave-swash interactions observed in the field for irregular waves (Chardón-Maldonado et al., 2016). Chen et al. (2023), in their recent extensive review of sediment transport models, concluded that even though there is an acceptance that wave-swash interactions play a critical role in the sediment transport in the swash zone, there are no parameters to determine the interaction type or the resulting sediment transport.

Interest in wave-swash interactions also stems from the observations that suggest wave-swash interactions could develop vertical (non-hydrostatic) pressure gradients and associated accelerations that trigger sediment liquefaction in the surf and swash zones (Elfrink & Baldock, 2002; Puleo & Butt, 2006; Puleo & Torres-Freyermuth, 2016; Florence et al., 2022; Stark et al., 2022), which would then lead to large sediment transport events. However, no framework exists for predicting when and if such liquefaction occurs. Indeed, some field observations suggest that wave-swash interactions that seem to follow very similar flow patterns produce sediment transport in opposite directions (Masselink et al., 2009). Similarly, output of numerical models for predicting beach morphology changes [e.g., Smit et al. (2010)], when compared with controlled laboratory experiments, show that while the hydrodynamic variables are well predicted, the suspended sediment concentrations are not, especially during wave-swash interactions (Ruffini et al., 2020; Mancini et al., 2021). Thus, even when sediment transport mechanisms such as bedload and suspended sediment transport are implemented, they appear to lack important aspects of the flow and acceleration.

In this work, we use controlled experiments in a wave flume to find quantitative descriptions of wave-swash interactions. Our method considers the generation solitary waves since they travel without change of form [ignoring small viscous losses (Liu et al., 2007)] and generate large swash events whose properties can be understood in terms of a small set of input parameters (Pujara et al., 2015b). By generating two consecutive solitary wave events, we can set the strength of the first swash event through the wave height of the first wave and set the wave height and arrival time of the second wave through its height and separation from the first wave, thereby providing full control of the wave-swash interaction. This approach complements previous experiments using regular waves, bi-chromatic waves, solitary waves, and dam-break bores to understand and flow and transport in the swash zone (Alsina et al., 2009; O'Donoghue et al., 2010; Sou & Yeh, 2011; Alsina et al., 2012; Kikkert et al., 2012; Lo et al., 2013; Pujara et al., 2015a; Alsina et al., 2016; O'Donoghue et al., 2016; Alsina et al., 2018; Wu et al., 2021; Barranco & Liu, 2021; Pintado-Patiño et al., 2021). By mimicking the interactions observed in the field, we analyze the main kinematic properties of wave-swash interactions, focusing in particular on the vertical accelerations and their correlation with the flow evolution. We find that there are large upward-directed vertical accelerations for certain interactions that cluster together when mapped onto two dimensionless parameters that can also predict different wave-swash interaction types.

The remainder of this manuscript is structured as follows. Section 2 presents the description of the experimental setup, including wave generation and instrumentation, section 3 contains the results and analysis for swash events driven by single solitary waves
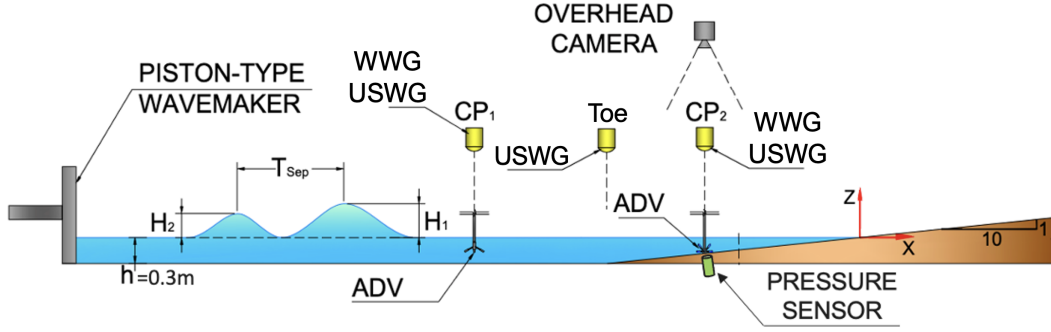
Figure 1. Wave flume definition sketch with locations of the different sensors.

¹¹⁵ and wave-swash interactions driven by consecutive solitary waves, and the concluding
¹¹⁶ remarks are given in section 4.

2 Laboratory Experiments

2.1 Wave Flume Setup

¹¹⁹ Experiments were conducted in a wave flume at the Water Science and Engineer-
¹²⁰ ing Laboratory (WSEL) of the University of Wisconsin-Madison (Figure 1). The WSEL
¹²¹ flume (39 m length, 0.9 m width, and 1.1 m height) is equipped with a piston-type wave-
¹²² maker controlled by AwaSys (Aalborg University, Denmark) at one end and an imper-
¹²³ meable smooth beach with slope 1:10 at the other end. The water depth was kept con-
¹²⁴ stant throughout the experiments at $h = 0.3$ m. Swash events and wave-swash events
¹²⁵ were generated using solitary waves. We place the origin of the lab coordinate system
¹²⁶ at the still water line (SWL) on the beach with x pointing onshore and z pointing up-
¹²⁷ wards against gravity.

¹²⁸ Measurements of both the free-surface displacement (η and the flow velocity (u, v, w)
¹²⁹ were taken at two control points, one in a constant depth at $x = -8.83$ m (CP$_1$) and
¹³⁰ one in the wave-swash interaction zone at $x = -0.3$ m (CP$_2$), and additional measure-
¹³¹ ments of the free-surface displacement were taken at the toe of the beach ($x = -3$ m).
¹³² The free-surface displacement was measured at CP$_1$ and CP$_2$ using ultrasonic acoustic
¹³³ wave gauges (USWG; Senix ToughSonic-3 with 1 mm accuracy) and wire wave gauges
¹³⁴ (WWG, HR Wallingford with 0.1 mm accuracy) whereas only an ultrasonic wave gauge
¹³⁵ was used at the beach toe. The WWG calibration is prone to drift and thus the WWGs
¹³⁶ were calibrated at the start of every day when experiments were run whereas the USWG
¹³⁷ calibration is much more stable and only required calibration once before the start of the
¹³⁸ experiments. While both sensor types can be expected to give reliable data in the off-
¹³⁹ shore regions where the wave slopes are mild, the WWG has better accuracy and is able
¹⁴⁰ to reliably measure the free-surface displacement with steep wave slopes due to wave break-
¹⁴¹ ing at CP$_2$ that the USWG is unable to measure. However, the WWG has a non-linear
¹⁴² calibration response for shallow depths $((\eta + h_{\mathrm{CP}_2}) \leq 2$ cm), and we remove data be-
¹⁴³ low this threshold water depth. In the analysis below, we use the WWG data at CP$_1$
¹⁴⁴ and CP$_2$ and the USWG data at the beach toe.

¹⁴⁵ Acoustic Doppler velocimeters (ADVs, Nortek Vectrino Plus with accuracy of 1%
¹⁴⁶ FS) were used to measure all three components of the flow velocity at CP$_1$ (down-looking
¹⁴⁷ probe) and CP$_2$ (side-looking probe) with their sampling volumes positioned at 15 cm
¹⁴⁸ and 0.75 cm above the bed, respectively. For data quality and control, we only report
¹⁴⁹ data with a signal-to-noise ratio (SNR) greater than 12 and a correlation value (CORR)
¹⁵⁰ greater than 70. Finally, at CP$_2$, a custom pressure transducer (Omega PX409 series with

accuracy of 0.08% FS) was installed with the sensor face flush with the beach surface to measure the bed pressure and two overhead cameras (JAI GO-5100-USB, 2464 x 2056 px, 8 bit resolution) fitted with 8 mm lenses (Thor labs) were mounted above the flume to record images over a combined field of view (FOV) of $x = [-70, 10]$ cm at 33.3 Hz. Data collection from all instruments were synchronized with the start of the wave paddle motion.

2.2 Wave Conditions

Single and consecutive solitary waves were used in the experiments to generate single swash events and wave-swash interaction events, respectively. The wave paddle trajectory for single solitary waves uses Goring's theory (Goring, 1979), but the paddle trajectory for consecutive solitary waves was calculated by AwaSys using Boussinesq wave-maker theory backward in time to create the desired free-surface elevation timeseries at a specified location. As an input to this system, we constructed a timeseries of consecutive solitary waves to be realised at CP_1 using the Boussinesq solution for solitary waves (Boussinesq, 1872) with the wave peaks separated by a nominal separation time, T_{sep}. Measurements of the free-surface displacement and flow velocity at CP_1 compared well with the Boussinesq solution, which showed that the wave generation was robust for producing single and consecutive solitary waves. Additionally, we assessed the experimental repeatability by repeating specific cases covering different wave-swash interaction types five times, which showed the data were very repeatable, as has been previously observed in these type of experiments (Pujara et al., 2015a).

The final set of wave conditions covered single solitary waves with wave heights $H = [0.1, 0.2, 0.3, 0.4]h$ and consecutive solitary waves with $H_{1,2} = [0.1, 0.2, 0.3, 0.4]h$ and $T_{sep} = [0.75, 1.0, 1.25, 1.50, 1.75, 2.0]T_{H_1}$ where H_1 is the wave height for the first wave, H_2 is the wave height for the second wave, and T_{H_1} is the (effective) wave period of the first wave. There are four cases of single solitary waves and 60 cases of consecutive solitary waves (summarized in Table 1 below).

2.3 Vertical Accelerations

We inferred the (total) vertical accelerations at CP_2 using data of the bed pressure and surface elevation. To do so, we start with the vertical component of the Navier-Stokes equation

$$\frac{Dw}{Dt} = -\frac{1}{\rho}\frac{\partial p}{\partial z} - g + \nu\nabla^2 w, \tag{1}$$

where w is the velocity in the z (vertical) direction, g is the gravitational acceleration, ρ is the fluid density, and ν is the kinematic viscosity. The viscous term ($\nu\nabla^2 w$) was neglected under the assumptions that its influence is small over the bulk of the water column except in thin boundary layers adjacent to the bed and the free surface. Next, assuming that the pressure varied linearly with depth in the shallow swash flow at CP_2, the vertical pressure gradient was approximated in terms of the difference between the surface pressure and bed pressure. Together, these assumptions reduce Eq. 1 to

$$\frac{Dw}{Dt} \approx -\frac{1}{\rho}\frac{(p_{surface} - p_{bed})}{(\eta + h_{CP_2})} - g = \frac{p_{bed}}{\rho(\eta + h_{CP_2})} - g, \tag{2}$$

where $p_{surface} = 0$ in gauge pressure, p_{bed} is the bed pressure, and $(\eta + h_{CP_2})$ is the total local water depth at CP_2. Thus, we can infer the total vertical accelerations from simultaneous measurements of the total water depth and the bed pressure. Note, only non-hydrostatic pressure distributions lead to vertical accelerations since the vertical acceleration vanishes ($Dw/Dt = 0$) if the pressure distribution is hydrostatic ($p_{bed} = \rho g(\eta + h_{CP_2})$).
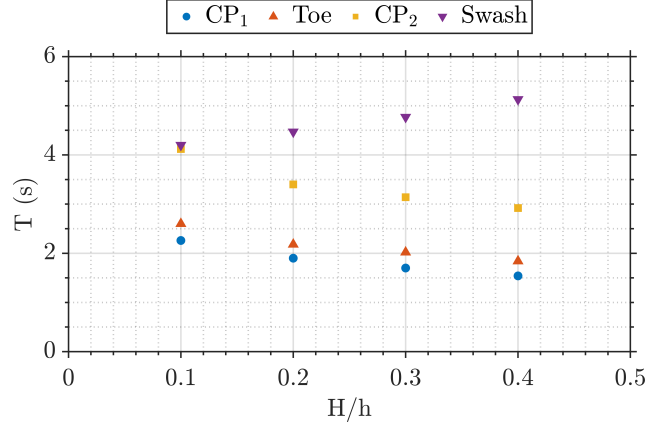
Figure 2. Wave periods measured at different locations along the flume. See main text for explanation of how the period at each location was found.

3 Results

3.1 Single Solitary Wave

We use the results of single solitary wave experiments to extract information of single swash events that can be used as a baseline to understand the wave-swash events driven by consecutive solitary waves. Figure 2 shows data of the wave period measured at different cross-shore locations for single solitary wave experiments. At CP_1, beach toe, and CP_2, the wave period is estimated as the time over which the free-surface displacement timeseries is above a small threshold (2.5 mm for $H/h = [0.1, 0.2, 0.3]$ and 4 mm for $H/h = 0.4$). In the constant depth region, beach toe, and at CP_2, the period decreases with increasing wave height. This decrease can be understood in terms of the mechanics of solitary waves, where the wave height and the wavelength are linked. In particular, it is well known that solitary waves become narrower as the wave height increases (Madsen et al., 2008).

These results of decreasing wave period with increasing wave height are counter intuitive for the swash event. We expected, and observed, that waves of larger wave height generated larger swash events that reached a higher run-up and took longer to complete the uprush-backwash swash cycle. Thus, it is clear that the wave periods measured offshore of the SWL do not provide a good measure of the period of the swash event. To estimate the true swash period, we used the camera images to find the time between when the shoreline at the still water line first begins to move during the uprush to when a hydraulic jump begins to form during the downrush. This swash period, shown in Figure 2, supports basic intuition and observations: the swash period increases with incident wave height. This result also underscores the importance of measuring the swash period directly. In the analysis of wave-swash interactions presented below, we emphasise the importance of this swash period, T_{swash}. In particular, the quantity $T_{\text{sep}}/T_{\text{swash}}$ is the dynamically important dimensionless separation time between consecutive swash events.

Figure 3 shows the upward-directed peak vertical accelerations measured at CP_2 (as described in Sec. 2.3) for single solitary wave experiments as a function of wave height. These peak vertical accelerations occur before the wave crest during the passage of the wave front. As wave height increases, we observe larger vertical accelerations with values close to gravity for the largest wave tested. The Boussinesq theory of solitary waves allows us to predict how the maximum vertical acceleration varies with the wave height in the constant depth region. It is easily shown that the peak vertical acceleration fol-
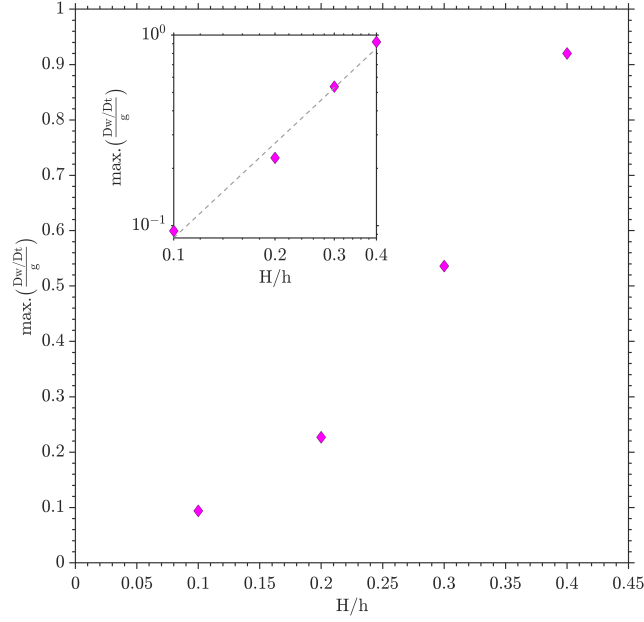
Figure 3. Peak upward-directed vertical accelerations at CP_2 as a function of incident solitary wave height. Inset shows the same data with a power-law fit where the best-fit power law exponent is found to be 1.65.

lows $Dw/Dt \sim (H/h)^{3/2}$ to leading order and that this scaling comes from the local time derivative $(\partial w/\partial t)$ which dominates over the advective acceleration $(\mathbf{u} \cdot \nabla w)$. The inset in Figure 3 shows that the peak vertical acceleration at CP_2 follows a power law with a power-law exponent that is empirically found to be 1.65. The similarity of this value with the predicted value of 1.5 using solitary wave theory in constant depth suggests the peak vertical accelerations for wave crests during their climb of a sloping beach can be understood in terms of incident wave properties, even up to very shallow water depths where the wave shape has evolved significantly during shoaling. It also suggests that shoaling of a wave crest in otherwise quiescent water is insufficient to generate vertical accelerations that exceed gravity.

3.2 Consecutive Solitary Waves

3.2.1 Wave-swash Interaction Types and Interaction Zones

By using consecutive solitary waves where we can control the height of each wave and the separation between them, we were able to produce different wave-swash interactions types as observed, categorised, and described by (Hughes & Moseley, 2007) and others in the field. These are wave-uprush interaction (WUI), where the second wave crest has delayed breaking and collapse as it propagates further onshore over a layer of uprush flow generated by the swash of the first wave crest; weak wave-backwash interaction (WWBI), where the second wave crest encounters the backwash flow of the swash of the first wave, inducing accelerated breaking and collapse; and strong wave-backwash interaction (SWBI), where a stationary bore is generated by sudden breaking of the second wave crest as it encoutners the strong backwash flow of the swash of the first wave.

Table 1 presents a complete list of the 60 cases of consecutive solitary wave experiments. For each case, we list the observed wave-swash interaction type, the wave height ratio (H_2/H_1) measured at the beach toe and at CP_2 and the dimensionless separation

Table 1. Experimental cases, wave parameters, characteristic ratios at different locations, and type of interaction observed. The interaction types, as described by Hughes and Moseley (2007), include wave-uprush interaction (WUI), weak wave-backwash interaction (WWBI), and strong wave-backwash interaction (SWBI)

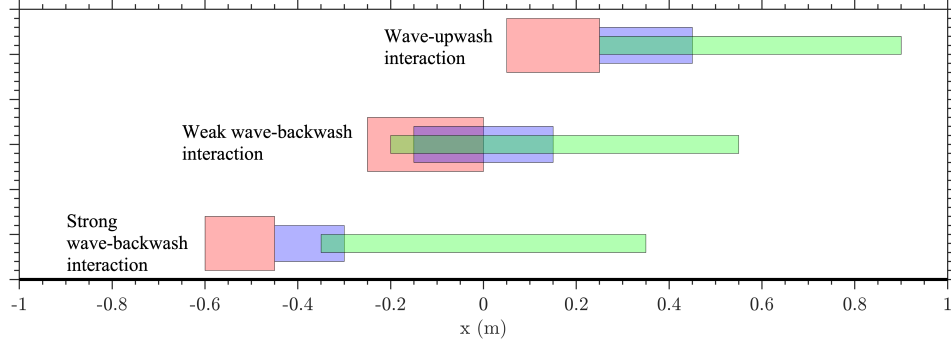| Cases	$(H_2/H_1)_{\text{toe}}$	$(T_{\text{sep}}/T_{\text{swash}})_{\text{toe}}$	$(H_2/H_1)_{\text{CP}_2}$	$(T_{\text{sep}}/T_{\text{swash}})_{\text{CP}_2}$	Type
$H_1 = 0.1h; H_2 = 0.4h; T_{\text{sep}} = 0.75T_{H_1}$	3.2	0.4	3.2	0.3	WUI
$H_1 = 0.2h; H_2 = 0.3h; T_{\text{sep}} = 0.75T_{H_1}$	1.4	0.3	3.3	0.5	WUI
$H_1 = 0.2h; H_2 = 0.4h; T_{\text{sep}} = 0.75T_{H_1}$	1.7	0.3	3.4	0.8	WUI
$H_1 = 0.2h; H_2 = 0.4h; T_{\text{sep}} = 1.00T_{H_1}$	1.8	0.4	1.8	1.0	WUI
$H_1 = 0.3h; H_2 = 0.3h; T_{\text{sep}} = 0.75T_{H_1}$	1.0	0.3	1.8	1.2	WUI
$H_1 = 0.3h; H_2 = 0.4h; T_{\text{sep}} = 0.75T_{H_1}$	1.2	0.3	2.3	1.4	WUI
$H_1 = 0.3h; H_2 = 0.4h; T_{\text{sep}} = 1.00T_{H_1}$	1.3	0.4	1.5	0.4	WUI
$H_1 = 0.4h; H_2 = 0.3h; T_{\text{sep}} = 0.75T_{H_1}$	0.8	0.3	1.6	0.6	WUI
$H_1 = 0.4h; H_2 = 0.4h; T_{\text{sep}} = 0.75T_{H_1}$	1.0	0.3	1.5	0.7	WUI
$H_1 = 0.4h; H_2 = 0.4h; T_{\text{sep}} = 1.00T_{H_1}$	1.1	0.3	1.5	0.9	WUI
$H_1 = 0.1h; H_2 = 0.4h; T_{\text{sep}} = 1.00T_{H_1}$	3.3	0.6	0.7	1.1	WWBI
$H_1 = 0.1h; H_2 = 0.4h; T_{\text{sep}} = 1.25T_{H_1}$	3.4	0.9	0.6	1.2	WWBI
$H_1 = 0.2h; H_2 = 0.2h; T_{\text{sep}} = 0.75T_{H_1}$	1.1	0.4	1.7	0.3	WWBI
$H_1 = 0.2h; H_2 = 0.2h; T_{\text{sep}} = 1.00T_{H_1}$	1.1	0.6	1.9	0.5	WWBI
$H_1 = 0.2h; H_2 = 0.2h; T_{\text{sep}} = 1.25T_{H_1}$	1.1	0.7	1.9	0.6	WWBI
$H_1 = 0.2h; H_2 = 0.3h; T_{\text{sep}} = 1.00T_{H_1}$	1.5	0.5	1.8	0.8	WWBI
$H_1 = 0.2h; H_2 = 0.3h; T_{\text{sep}} = 1.25T_{H_1}$	1.5	0.6	1.7	0.9	WWBI
$H_1 = 0.2h; H_2 = 0.3h; T_{\text{sep}} = 1.50T_{H_1}$	1.5	0.8	0.7	1.1	WWBI
$H_1 = 0.2h; H_2 = 0.4h; T_{\text{sep}} = 1.25T_{H_1}$	2.2	0.5	1.9	0.3	WWBI
$H_1 = 0.2h; H_2 = 0.4h; T_{\text{sep}} = 1.50T_{H_1}$	1.8	0.7	2.1	0.4	WWBI
$H_1 = 0.2h; H_2 = 0.4h; T_{\text{sep}} = 1.75T_{H_1}$	2.1	0.8	2.1	0.5	WWBI
$H_1 = 0.3h; H_2 = 0.2h; T_{\text{sep}} = 0.75T_{H_1}$	0.8	0.4	2.1	0.7	WWBI
$H_1 = 0.3h; H_2 = 0.2h; T_{\text{sep}} = 1.00T_{H_1}$	0.8	0.5	1.9	0.8	WWBI
$H_1 = 0.3h; H_2 = 0.2h; T_{\text{sep}} = 1.25T_{H_1}$	0.8	0.6	1.3	1.0	WWBI
$H_1 = 0.3h; H_2 = 0.3h; T_{\text{sep}} = 1.00T_{H_1}$	1.1	0.4	1.2	0.4	WWBI
$H_1 = 0.3h; H_2 = 0.3h; T_{\text{sep}} = 1.25T_{H_1}$	1.1	0.5	1.2	0.5	WWBI
$H_1 = 0.3h; H_2 = 0.3h; T_{\text{sep}} = 1.50T_{H_1}$	1.1	0.6	1.3	0.7	WWBI
$H_1 = 0.3h; H_2 = 0.4h; T_{\text{sep}} = 1.25T_{H_1}$	1.4	0.5	1.0	0.8	WWBI
$H_1 = 0.3h; H_2 = 0.4h; T_{\text{sep}} = 1.50T_{H_1}$	1.3	0.6	0.9	0.9	WWBI
$H_1 = 0.3h; H_2 = 0.4h; T_{\text{sep}} = 1.75T_{H_1}$	1.3	0.7	0.6	1.0	WWBI
$H_1 = 0.3h; H_2 = 0.4h; T_{\text{sep}} = 2.00T_{H_1}$	1.3	0.8	1.4	0.3	WWBI
$H_1 = 0.4h; H_2 = 0.2h; T_{\text{sep}} = 0.75T_{H_1}$	0.6	0.4	1.4	0.4	WWBI
$H_1 = 0.4h; H_2 = 0.2h; T_{\text{sep}} = 1.00T_{H_1}$	0.6	0.5	1.5	0.5	WWBI
$H_1 = 0.4h; H_2 = 0.2h; T_{\text{sep}} = 1.25T_{H_1}$	1.0	0.6	1.5	0.7	WWBI
$H_1 = 0.4h; H_2 = 0.3h; T_{\text{sep}} = 1.00T_{H_1}$	0.9	0.4	1.3	0.8	WWBI
$H_1 = 0.4h; H_2 = 0.3h; T_{\text{sep}} = 1.25T_{H_1}$	0.9	0.5	1.4	0.9	WWBI
$H_1 = 0.4h; H_2 = 0.3h; T_{\text{sep}} = 1.50T_{H_1}$	0.9	0.6	1.4	0.3	WWBI
$H_1 = 0.4h; H_2 = 0.3h; T_{\text{sep}} = 1.75T_{H_1}$	0.9	0.6	1.6	0.4	WWBI
$H_1 = 0.4h; H_2 = 0.4h; T_{\text{sep}} = 1.25T_{H_1}$	1.1	0.4	1.6	0.5	WWBI
$H_1 = 0.4h; H_2 = 0.4h; T_{\text{sep}} = 1.50T_{H_1}$	1.1	0.5	1.7	0.6	WWBI
$H_1 = 0.4h; H_2 = 0.4h; T_{\text{sep}} = 1.75T_{H_1}$	1.1	0.6	1.5	0.7	WWBI
$H_1 = 0.4h; H_2 = 0.4h; T_{\text{sep}} = 2.00T_{H_1}$	1.1	0.7	1.4	0.8	WWBI
$H_1 = 0.1h; H_2 = 0.4h; T_{\text{sep}} = 1.50T_{H_1}$	3.4	1.1	1.0	0.4	SWBI
$H_1 = 0.2h; H_2 = 0.2h; T_{\text{sep}} = 1.50T_{H_1}$	1.1	0.9	1.1	0.5	SWBI
$H_1 = 0.2h; H_2 = 0.2h; T_{\text{sep}} = 1.75T_{H_1}$	1.1	1.0	1.0	0.6	SWBI
$H_1 = 0.2h; H_2 = 0.2h; T_{\text{sep}} = 2.00T_{H_1}$	1.2	1.2	0.8	0.7	SWBI
$H_1 = 0.2h; H_2 = 0.3h; T_{\text{sep}} = 1.75T_{H_1}$	1.5	0.9	0.9	0.8	SWBI
$H_1 = 0.2h; H_2 = 0.3h; T_{\text{sep}} = 2.00T_{H_1}$	1.6	1.1	0.9	0.9	SWBI
$H_1 = 0.2h; H_2 = 0.4h; T_{\text{sep}} = 2.00T_{H_1}$	1.9	1.0	1.2	0.3	SWBI
$H_1 = 0.3h; H_2 = 0.2h; T_{\text{sep}} = 1.50T_{H_1}$	0.8	0.7	1.2	0.4	SWBI
$H_1 = 0.3h; H_2 = 0.2h; T_{\text{sep}} = 1.75T_{H_1}$	0.8	0.8	1.2	0.5	SWBI
$H_1 = 0.3h; H_2 = 0.2h; T_{\text{sep}} = 2.00T_{H_1}$	0.8	0.9	1.3	0.6	SWBI
$H_1 = 0.3h; H_2 = 0.3h; T_{\text{sep}} = 1.75T_{H_1}$	1.1	0.7	1.1	0.7	SWBI
$H_1 = 0.3h; H_2 = 0.3h; T_{\text{sep}} = 2.00T_{H_1}$	1.1	0.9	0.9	0.8	SWBI
$H_1 = 0.4h; H_2 = 0.2h; T_{\text{sep}} = 1.50T_{H_1}$	0.7	0.6	1.2	0.3	SWBI
$H_1 = 0.4h; H_2 = 0.2h; T_{\text{sep}} = 1.75T_{H_1}$	1.1	0.8	1.4	0.3	SWBI
$H_1 = 0.4h; H_2 = 0.2h; T_{\text{sep}} = 2.00T_{H_1}$	0.6	0.8	1.3	0.4	SWBI
$H_1 = 0.4h; H_2 = 0.3h; T_{\text{sep}} = 2.00T_{H_1}$	0.9	0.7	1.4	0.5	SWBI
$H_1 = 0.1h; H_2 = 0.4h; T_{\text{sep}} = 1.75T_{H_1}$	3.6	1.3	1.3	0.6	No Interaction
$H_1 = 0.1h; H_2 = 0.4h; T_{\text{sep}} = 2.00T_{H_1}$	3.6	1.5	1.1	0.7	No Interaction

Figure 4. Spatial extent of wave-swash interactions and their different stages: jet slamming (red), splash-induced flow (purple), and fully 3D turbulent flow (green). Wave-upwash interaction (H_1=0.2h ; H_2=0.4h ; T_{sep}=1.0T_{H_1}); weak wave-backwash interaction (H_1=0.3h ; H_2=0.3h ; T_{sep}=1.5T_{H_1}); and strong wave-backwash interaction (H_1=0.3h ; H_2=0.2h ; T_{sep}=1.5T_{H_1}).

time (T_{sep}/T_{swash}) measured at CP_2. The wave height and separation time measurements were made by first using a Gaussian kernel low pass filter (Mordant et al., 2004; Pujara et al., 2021) to the surface elevation measurements to reduce noise and simplify finding the peak of the free-surface displacement signal.

Figure 4 maps out the typical stages of a wave-swash interaction with examples of each interaction type. From the camera images, we observed that wave-swash interactions consistently displayed three stages: First, the approaching wave crest's overturning created a jet which struck the water ahead of it ("jet slamming"). Second, this breaker jet created a splash that altered the shallow flow ahead of the breaker ("splash-induced flow"). Finally, this interaction between the breaker and the swash of the preceding wave showed signs of fluid instabilities that quickly transitioned into highly turbulent flow ("fully 3D turbulent flow"). Some aspects of these observations have also been reported in the inner surf and swash zones of plunging breaker regular waves (Sou & Yeh, 2011; Sumer et al., 2013). However, the location of where the interaction takes place, as well as the spatial extent where these three stages occur, varies for different wave-swash interaction types, which has not been previously reported in laboratory studies. As Figure 4 shows, the interaction zone moves offshore for wave-backwash interactions compared with wave-uprush interactions and there is less overlap in the spatial extent of the three stages for strong wave-backwash interactions compared with weak wave-backwash interactions.

3.2.2 Hydrodynamics of Wave-swash Interactions

While the qualitative wave-swash interaction types and stages described above are useful for classification purposes, they do not reveal any information of the underlying hydrodynamics. Thus, we now tackle the quantitative analysis of wave-swash interactions. Figures 5, 6, and 7 show the typical timeseries at CP_2 for wave-upwash, weak wave-backwash, and strong wave-backwash interactions, respectively. Gaps in the data are related to quality control procedures described in Sec. 2.1. In the bed pressure data, there are large fluctuations after the passage of the first wave crest. These are associated with beach vibrations induced by the jet slamming of the first wave and are therefore experimental artefacts.

The top panels in these figures show the total water depth and bed pressure in units of depth together, which when compared with the vertical accelerations in the middle panel, show how the vertical accelerations result from a non-hydrostatic pressure distribution. Focusing on the vertical accelerations, it is evident that the passage of a shoal-
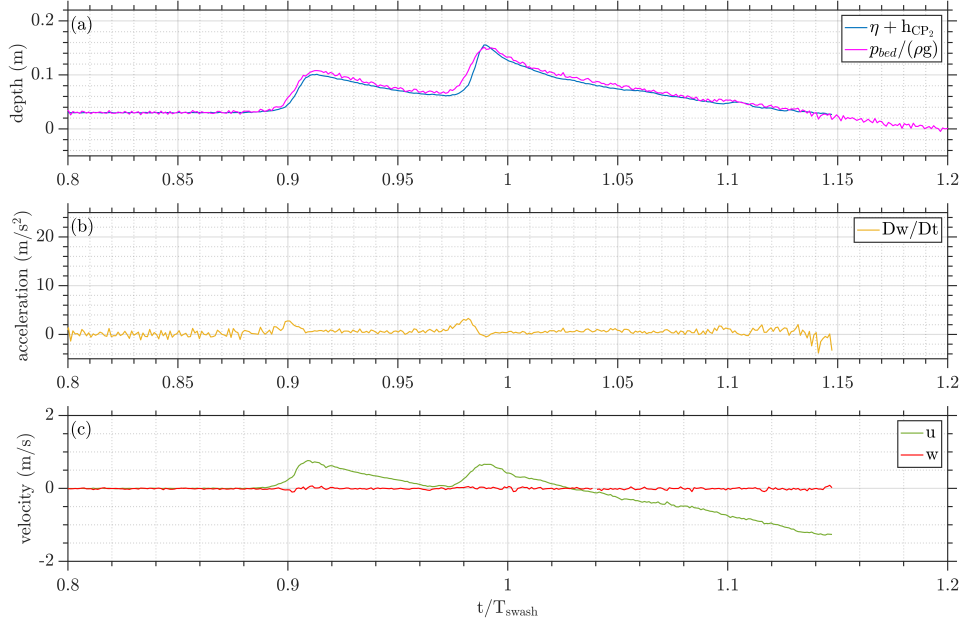
Figure 5. Time series of elevations, bottom pressures converted to elevations, and estimated total vertical accelerations. Wave-upwash interactions. Case: $H_1=0.2h$; $H_2=0.3h$; $T_{\mathrm{sep}}=0.75T_{H_1}$ ($H_2/H_1=1.5$, $T_{\mathrm{sep}}=0.084T_{\mathrm{swash}}$).
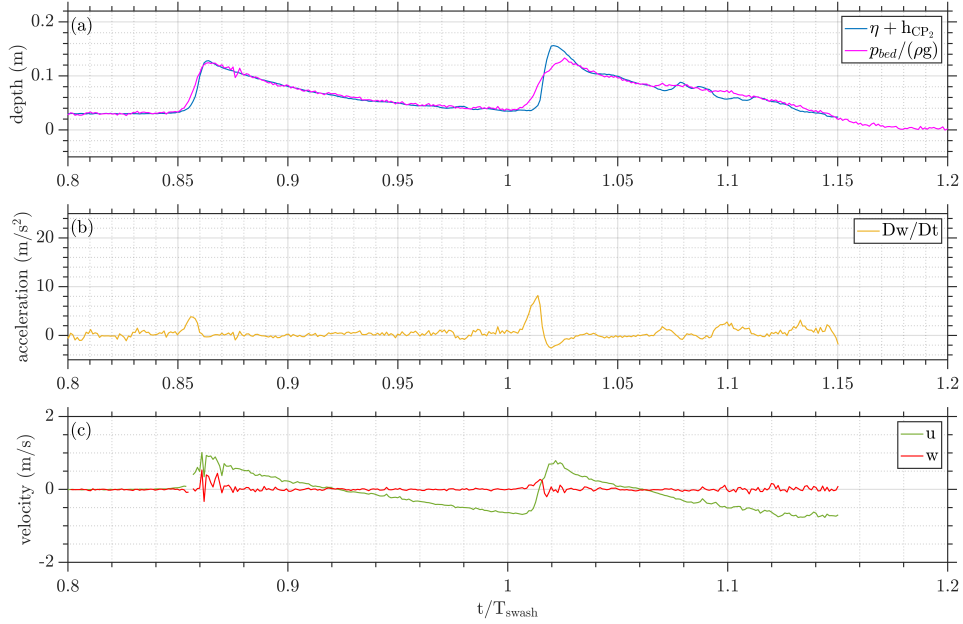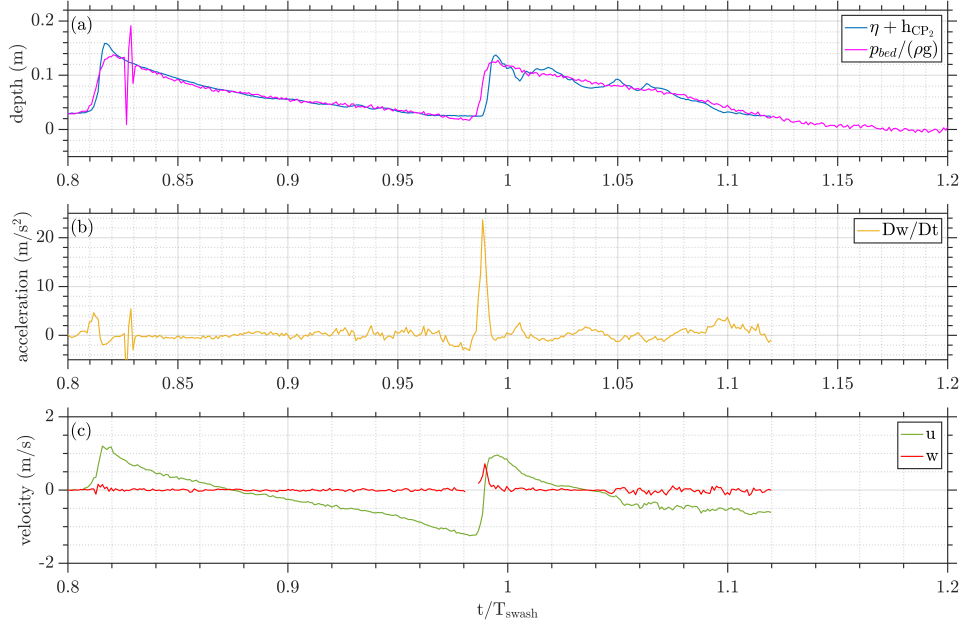

Figure 6. Time series of elevations, bottom pressures converted to elevations, and estimated total vertical accelerations. Weak wave-backwash interactions. Case: $H_1=0.3h$; $H_2=0.2h$; $T_{\mathrm{sep}}=1.25T_{H_1}$ ($H_2/H_1=0.667$, $T_{\mathrm{sep}}=0.128T_{\mathrm{swash}}$).

Figure 7. Time series of elevations, bottom pressures converted to elevations, and estimated total vertical accelerations. Strong wave-backwash interactions. Case: $H_1=0.4h$; $H_2=0.2h$; $T_{sep}=1.50T_{H_1}$ ($H_2/H_1=0.5$, $T_{sep}=0.137T_{swash}$).

ing wave crest into quiescent water generates accelerations of magnitude up to that of gravity, whereas the a wave crest interacting with the swash event of the previous wave results in larger acceleration with values far exceeding gravity. The velocity data in the bottom panel shows that the peak vertical acceleration in the wave-swash interaction is near concurrent with the peak positive horizontal and vertical velocities. Though we don't show it explicitly, the velocity data also show that, in contrast to single solitary wave data, the local time derivative of the vertical velocity ($\partial w/\partial t$) is insufficient to explain the inferred vertical accelerations, suggesting that the advective part of the vertical acceleration ($\mathbf{u} \cdot \nabla w$) is important. Finally, we note that the qualitative wave-swash interaction types do not necessarily predict the hydrodynamics, but the advantage of our experimental setup is that the wave height ratio H_2/H_1 and the dimensionless separation time T_{sep}/T_{swash} provide a quantitative parameter space in which we can map out the hydrodynamics.

Figure 8 shows the distribution of the wave-swash interactions as a function of H_2/H_1 and T_{sep}/T_{swash} as measured at the beach toe (panel a) and CP_2 (panel b). Satisfyingly, the observed qualitative interaction types cluster together: Wave-uprush interactions are towards the top (and slightly left), weak wave-backwash interactions are in the middle, and strong wave-backwash interactions are towards the bottom (and slightly right). The differences between the panels, which are driven by the location where the wave heights and separation time are measured, are also instructive. Based on the 'far field' measurements at the beach toe, it appears that the separation time between consecutive wave crests is more important for predicting the interaction type than the wave height ratio. In contrast, for values of $H_2/H_1 < 1$, the 'local' measurements at CP_2 show that the interactions are almost exclusively of the strong wave-backwash type. Since our main interest is in understanding the flow and accelerations in the wave-swash interaction zone, the following analyses will focus on measurements from CP_2.
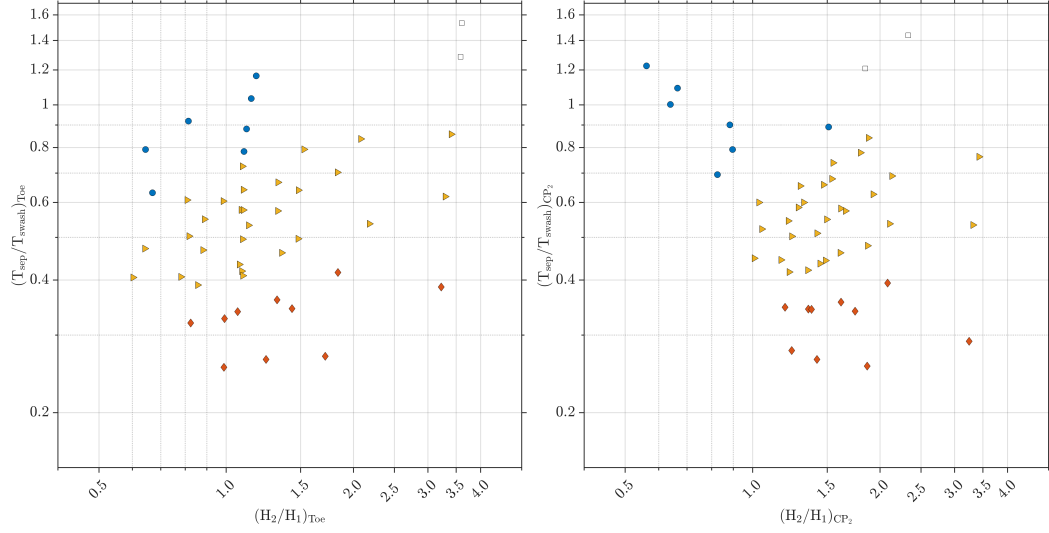
Figure 8. Wave-swash interactions mapping according to ratios H_2/H_1 and $T_{\mathrm{sep}}/T_{\mathrm{swash}}$. (a) Measurements at the toe of the beach. (b) Measurements at CP_2. Wave-upwash interaction (diamonds), weak wave-backwash interaction (triangles), strong wave-backwash interaction (circles), no interaction (blank squares).
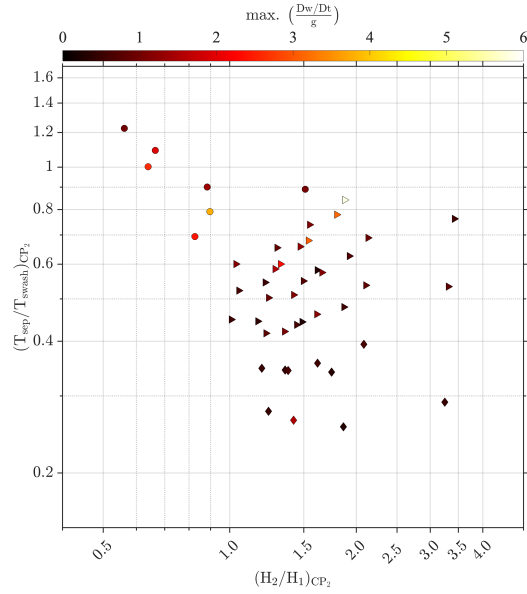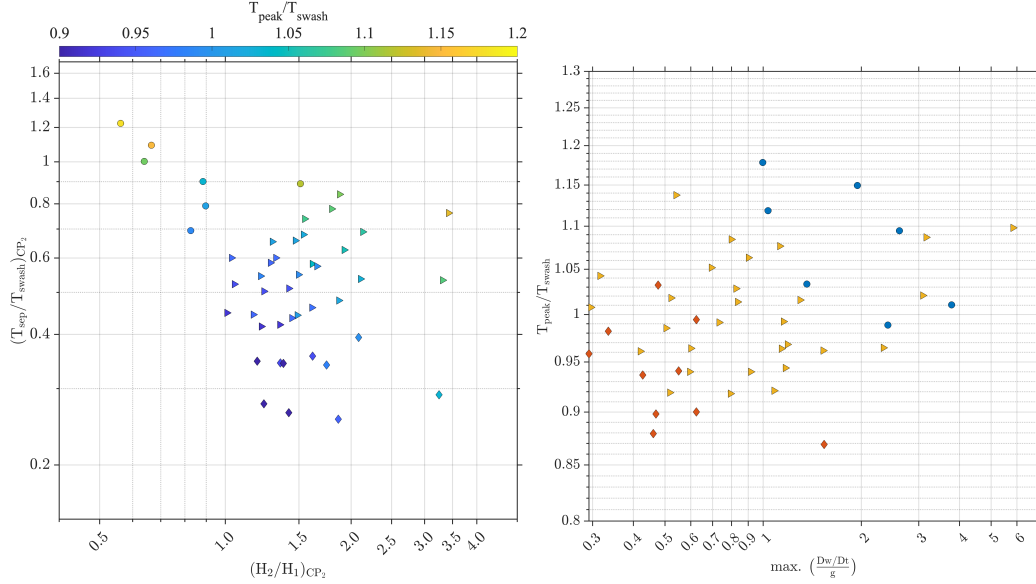

Figure 9. Distribution of maximum total vertical accelerations for different wave-swash interactions. Wave-upwash interaction (diamonds), weak wave-backwash interaction (triangles), strong wave-backwash interaction (circles).

Figure 10. Wave-swash interactions mapping. (a) Distribution of peak time for different wave interactions. (b) Maximum accelerations vs. $T_{\mathrm{peak}}/T_{\mathrm{swash}}$. Wave-upwash interaction (diamonds), weak wave-backwash interaction (triangles), strong wave-backwash interaction (circles).

Figure 9 presents the main results of this study: the peak upward-directed vertical acceleration magnitude as a function of H_2/H_1 and $T_{\mathrm{sep}}/T_{\mathrm{swash}}$ at CP_2. We observe that while the peak accelerations are larger for wave-backwash interactions (whether weak or strong) compared with wave-uprush interactions, it is not necessarily the case that strong wave-backwash interactions produce larger accelerations than weak wave-backwash interactions. The data show that there is a region of the parameter space, approximately $0.5 < H_2/H_1 < 2$ and $0.6 < T_{\mathrm{sep}}/T_{\mathrm{swash}} < 1.2$, where the peak accelerations are the largest. Physically, this corresponds to situations where the strength of the backwash flows generated by the swash of the first wave collide with an incoming wave front with approximately equal and opposite velocities. The peak vertical acceleration in the interaction is not particularly large if the velocity in either the backwash of the first wave or the wave front of the second wave dominates over the other.

In Figure 10, we investigate the time of the peak vertical acceleration, T_{peak}, to understand how it relates to the swash period T_{swash} and the magnitude of the acceleration peak. The timing of the peak is not necessarily solely dependent on T_{sep} (panel a), but the largest peak accelerations occur during the later stages of the swash flow associated with the first wave ($T_{\mathrm{peak}}/T_{\mathrm{swash}} \approx 1$) (panel b).

The final analysis relates to the correlations between the peak vertical accelerations and the flow velocities. Since our interest in vertical accelerations stems from the possibility of inducing large material suspension events, it is important to consider the direction and magnitude of the flow velocity at the same time since that will influence the speed and direction in which suspended material is advected. Figure 11 shows the velocity extracted at the time of peak vertical accelerations. The correlation between the peak vertical acceleration and the horizontal velocity is very weak, but interestingly, the vertical velocity at the time of peak vertical acceleration shows a (weak) positive correlation, suggesting that if large vertical accelerations destabilise a sediment bed or flush pore water with dissolved materials out of the bed, the flow field would act to transport that material upwards into the water column.
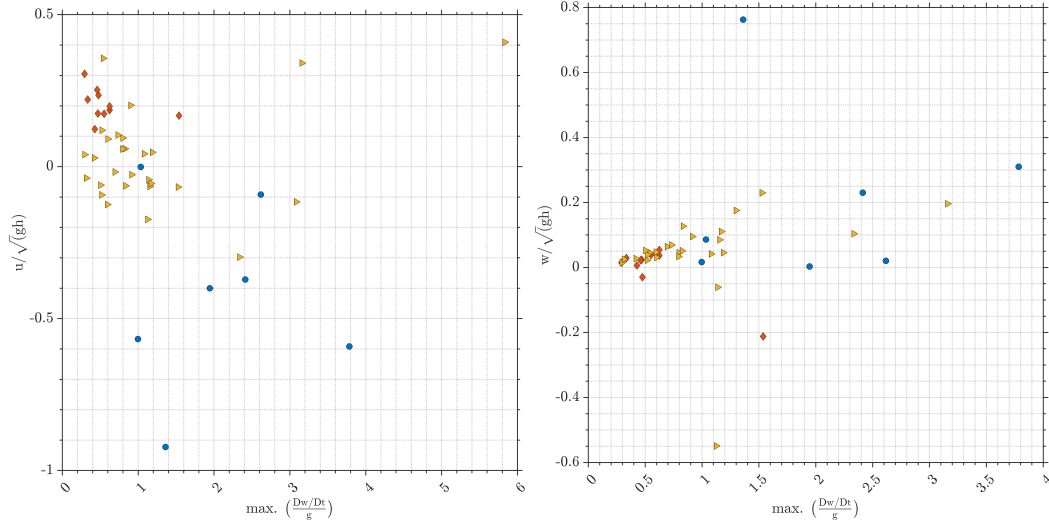
Figure 11. Distribution of wave-swash interactions for maximum total vertical accelerations and fluid velocities. (a) Horizontal velocity component. (b) Vertical velocity component. Wave-upwash interaction (diamonds), weak wave-backwash interaction (triangles), strong wave-backwash interaction (circles).
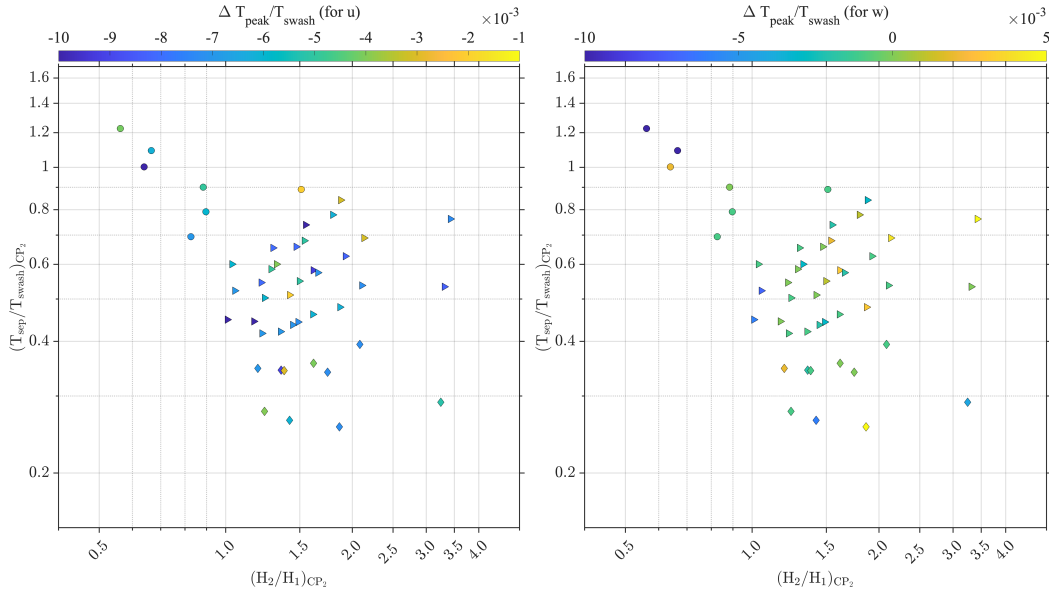

Figure 12. Time lag distribution between maximum total vertical accelerations and maximum velocities for different interactions. Positive values indicate that the peak positive velocity precedes the peak positive acceleration whereas negative values indicate that the peak acceleration precedes the peak velocity (a) Horizontal velocity component. (b) Vertical velocity component. Wave-upwash interaction (diamonds), weak wave-backwash interaction (triangles), strong wave-backwash interaction (circles).

While the fluid velocity at the time of the vertical acceleration peak is important, the timeseries data in Figures 5-7 also show that the peak positive horizontal and vertical velocities occur either shortly before or shortly after the peak acceleration. To quantify this, we calculate the time lag between the peak upward vertical acceleration and the peak positive fluid velocity for both components in Figure 12. Positive values indicate that the peak positive velocity precedes the peak positive acceleration whereas negative values indicate that the peak acceleration precedes the peak velocity. The results show that in most cases, the peak vertical acceleration precedes the peak positive (onshore directed) horizontal velocity, suggesting that even if there is not a strong correlation between the horizontal velocity and the vertical acceleration at the moment when the peak acceleration occurs, any material suspended into the water column by the vertical dynamics is prone to be transported onshore shortly after by the horizontal flow.

4 Concluding Remarks

In a set of controlled laboratory experiments, we used solitary waves to generate isloated single swash events (single solitary wave) and wave-swash interactions (consecutive solitary waves). By specifying the wave heights for consecutive solitary waves and the separation between them, it was possible to reproduce the wave-swash interactions found in the field, such as wave-upwash, weak wave-backwash, and strong wave-backwash interactions. The dimensionless parameters that control the wave-swash interactions in our experiments are the ratio of wave heights for consecutive solitary waves (H_2/H_1) and the time separation between them made dimensionless by the swash period of the first wave ($T_{\mathrm{sep}}/T_{\mathrm{swash}}$). When mapped onto this parameter space (H_2/H_1 vs. $T_{\mathrm{sep}}/T_{\mathrm{swash}}$), the different qualitative wave-swash interaction types formed distinct clusters, suggesting that these dimensionless parameters are sufficient to capture the observed variations in the field.

The main focus of the study was on the vertical accelerations, which were estimated from the differences between the depth measured with a surface wave gauge and the depth inferred from pressure measurements at the bed. While large vertical accelerations were associated with strong wave-backwash interactions, we found that weak wave-backwash interactions were associated with equally large vertical accelerations. The largest vertical accelerations were associated with wave-swash interactions that spanned $0.5 < H_2/H_1 < 2$ and $0.6 < T_{\mathrm{sep}}/T_{\mathrm{swash}} < 1.2$, where the vertical accelerations commonly exceeded gravity.

Finally, we analyzed the time lag between the maximum vertical acceleration and the maximum onshore horizontal and upward vertical velocity. The peak values of the vertical accelerations lead the peak onshore velocities and tend to be almost concurrent with the peak upward velocities. This suggests that wave-swash interactions may be an effective mechanism by which material such as sediment or solutes within sediment pores is suspended into the water column by the vertical dynamics before being advected onshore by the horizontal dynamics.

Overall, our findings show that non-hydrostatic effects, which are typically ignored in modelling coastal flows in the very shallow waters of the inner-surf and swash zones, are important in wave-swash interactions. Further, we hypothesize that these vertical accelerations are sufficient large such that they could lead to local liquefaction of sediment and hence produce large sediment transport events that may have an outsized influence on the net erosion or accretion of the beach foreshore region. Previous laboratory (Alsina et al., 2018) and field (Florence et al., 2022) studies have shown data of sediment suspension and transport consistent with this mechanism. Our framework of analysing isolated wave-swash interaction events, understanding their region of influence, and quantifying the vertical accelerations provide a framework with which to investigate the possiblity of sediment liquefaction and large sediment suspension events in the laboratory.

Future studies could investigate how these dynamics vary across the inner-surf and swash zones (our data is from a single control point) or include sediment to directly observe large sediment suspension events triggered by wave-swash interactions.

CRediT Author Statement

Availability Statement

The measured data, corresponding to time series of velocities, bottom pressures and surface elevations used for the analyses of flows and accelerations induced by wave-swash are available at https://github.com/cmezavalle/wave-swash-interactions. Version 1 of the MATLAB scripts used for the analyses and graphics generated in this work are preserved at https://github.com/cmezavalle/wave-swash-interactions. Data and codes are available via GNU General Public License v3.

Acknowledgments

References

Alsina, J. M., cáceres, I., Brocchini, M., & Baldock, T.   (2012).   An experimental study on sediment transport and bed evolution under different swash zone morphological conditions. *Coast. Eng.*, *68*, 31–43.

Alsina, J. M., Falchetti, S., & Baldock, T. E.   (2009).   Measurements and modelling of the advection of suspended sediment in the swash zone by solitary waves. *Coast. Eng.*, *56*, 621–631.

Alsina, J. M., Padilla, E. M., & Cáceres, I.   (2016).   Sediment transport and beach profile evolution induced by bi-chromatic wave groups with different group periods. *Coast. Eng.*, *114*, 325–340.

Alsina, J. M., van der Zanden, J., Cáceres, I., & Ribberink, J. S.   (2018).   The influence of wave groups and wave-swash interactions on sediment transport and bed evolution in the swash zone. *Coast. Eng.*, *140*, 23–42.

Baldock, T. E., & Holmes, P. (1999). Simulation and prediction of swash oscillations on asteep beach. *Coast. Eng.*, *36*, 219–242.

Barranco, I., & Liu, P. L.-F.   (2021).   Run-up and inundation generated by non-decaying dam-break bores on a planar beach. *J. Fluid Mech.*, *915*, A81:1-29.

Boussinesq, J.   (1872).   Théorie des ondes et des remous qui se propagent le long d'un canal rectangulaire horizontal, en communiquant au liquide contenu dans ce canal des vitesses sensiblement pareilles de la surface au fond.   *Journal de mathématiques pures et appliquées*, *17*, 55–108.

Brocchini, M., & Baldock, T. E.   (2008).   Recent advances in modeling swash zone dynamics: Influence of surf-swash interaction on nearshore hydrodynamics and morphodynamics. *Rev. Geophys.*, *46*, RG3003.

Chardón-Maldonado, P., Pintado-Patiño, J. C., & Puleo, J. A.   (2016).   Advances in swash-zone research: Small-scale hydrodynamic and sediment transport

processes. *Coast. Eng.*, *115*, 8–25.

Chen, W., van der Werf, J. J., & Hulscher, S. J. M. H. (2023). A review of practical models of sand transport in the swash zone. *Earth. Sci. Rev.*, *238*, 104355:1–17.

Dean, R. G., & Dalrymple, R. A. (2004). *Coastal processes with engineering applications.* Cambridge University Press.

Elfrink, B., & Baldock, T. (2002). Hydrodynamics and sediment transport in the swash zone: a review and perspectives. *Coast. Eng.*, *45*, 149–167.

Erikson, L., Larson, M., & Hanson, H. (2005). Prediction of swash motion and run-up including the effects of swash interaction. *Coast. Eng.*, *52*, 285–302.

Florence, M., Stark, N., Raubenheimer, B., & Elgar, S. (2022). Nearshore vertical pore pressure gradients and onshore sediment transport under tropical storm forcing. *J. Waterway, Port, Coastal, Ocean Eng.*, *148(6), 04022023*, 1–7.

Goring, D. G. (1979). *Tsunamis–the propagation of long waves onto a shelf.* Doctoral Thesis. California Institute of Technology.

Holthuijsen, L. H. (2007). *Waves in oceanic and coastal waters.* Cambridge University Press.

Hughes, M. G., & Moseley, A. S. (2007). Hydrokinematic regions within the swash zone. *Cont. Shelf. Res.*, *27*, 2000–2013.

Jackson, D. W. T., & Short, A. D. (2020). *Sandy beach morphodynamics.* Elsevier.

Kikkert, G. A., O'Donoghue, T., Pokrajac, D., & Dodd, N. (2012). Experimental study of bore-driven swash hydrodynamics on impermeable rough slopes. *Coast. Eng.*, *60*, 149–166.

Liu, P. L.-F., Park, Y. S., & Cowen, E. A. (2007). Boundary layer flow and bed shear stress under a solitary wave. *J. Fluid Mech.*, *574*, 449–463.

Lo, H.-Y., Park, Y. S., & Liu, P. L.-F. (2013). On the run-up and back-wash processes of single and double solitary waves — an experimental study. *Coast. Eng.*, *80*, 1–14.

Madsen, P. A., Fuhrman, D. R., & Schäffer, H. A. (2008). On the solitary wave paradigm for tsunamis. *J. Geophys. Res.*, *113*, C12012.

Mancini, G., Briganti, R., McCall, R., Dodd, N., & Zhu, F. (2021). Numerical modelling of intra-wave sediment transport on sandy beaches using a non-hydrostatic, wave-resolving model. *Ocean Dyn.*, *71(1)*, 1-20.

Mart´ınez, C., Contreras-Lopez, M., Winckler, P., Hidalgo, H., Godoy, E., & Agredano, R. (2018). Coastal erosion in central chile: A new hazard? *Ocean Coast. Manag.*, *156*, 141–155.

Masselink, G., Russell, P., Turner, I., & Blenkinsopp, C. (2009). Net sediment transport and morphological change in the swash zone of a high-energy sandy beach from swash event to tidal cycle time scales. *Mar. Geol.*, *267*, 18–35.

Mordant, N., Crawford, A. M., & Bodenschatz, E. (2004). Experimental lagrangian acceleration probability density function measurement. *Physica D*, *193*, 245–251. doi: 10.1016/j.physd.2004.01.041

O'Donoghue, T., Kikkert, G. A., andN. Dodd, D. P., & Briganti, R. (2016). Intra-swash hydrodynamics and sediment flux for dambreak swash on coarse-grained beaches. *Coast. Eng.*, *112*, 113–130.

O'Donoghue, T., Pokrajac, D., & Hondebrink, L. J. (2010). Laboratory and numerical study of dambreak-generated swash on impermeable slopes. *Coast. Eng.*, *57*, 513–530.

Pintado-Patiño, J. C., Puleo, J. A., Krafft, D., & Torres-Freyermuth, A. (2021). Hydrodynamics and sediment transport under a dam-break-driven swash: An experimental study. *Coast. Eng.*, *170*, 103986: 1–18.

Pujara, N., Clos, K. T. D., Ayres, S., Variano, E. A., & Karp-Boss, L. (2021). Measurements of trajectories and spatial distributions of diatoms (coscinodiscus spp.) at dissipation scales of turbulence. *Expt. Fluids*, *62*, 149. doi: 10.1007/s00348-021-03240-5

Pujara, N., Liu, P. L.-F., & Yeh, H. (2015b). The swash of solitary waves on a plane beach: flow evolution, bed shear stress and run-up. *J. Fluid Mech.*, *779*, 556–597.

Pujara, N., Liu, P. L.-F., & Yeh, H. H. (2015a). An experimental study of the interaction of two successive solitary waves in the swash: A strongly interacting case and a weakly interacting case. *Coast. Eng.*, *105*, 66–74.

Puleo, J. A., Beach, R. A., Holman, R. A., & Allen, J. S. (2000). Swash zone sediment suspension and transport and the importance of bore-generated turbulence. *J. Geophys. Res.*, *105*, 17,021-17,044.

Puleo, J. A., & Butt, T. (2006). The first international workshop on swash-zone processes. *Cont. Shelf Res.*, *26*, 556–560.

Puleo, J. A., & Torres-Freyermuth, A. (2016). The second international workshop on swash-zone processes. *Coast. Eng.*, *115*, 1–7.

Ruffini, G., Briganti, R., Alsina, J. M., Brocchini, M., Dodd, N., & McCall, R. (2020). Numerical modeling of flow and bed evolution of bichromatic wave groups on an intermediate beach using nonhydrostatic xbeach. *J. Waterway, Port, Coastal, Ocean Eng.*, *146(1), 04019034*, 1–17.

Smit, P., Stelling, G., Roelvink, D. J. A., van Thiel de Vries, J., McCall, R., van Dongeren, A., . . . Jacobs, R. (2010). *Xbeach: Non-hydrostatic model: Validation, verification and model description.* Deltares Technical Report.

Sou, I. M., & Yeh, H. (2011). Laboratory study of the cross-shore flow structure in the surf and swash zones. *J. Geophys. Res.*, *116, C03002*, 1–15.

Stark, N., Mewis, P., Reeve, B., Florence, M., Piller, J., & Simon, J. (2022). Vertical pore pressure variations and geotechnical sediment properties at a sandy beach. *Coast. Eng.*, *172, 104058*, 1–15.

Sumer, B. M., Guner, H., & Hansen, N. M. (2013). Laboratory observations of flow and sediment transport induced by plunging regular waves. *J. Geophys. Res.: Oceans*, *118*, 6161–6182. doi: 10.1002/jgrc.20450

Toimil, A., Camus, P., Losada, I. J., Cozannet, G. L., Nicholls, R. J., Idier, D., & Maspataud, A. (2020). Climate change-driven coastal erosion modelling in temperate sandy beaches: Methods and uncertainty treatment. *Earth-Science Reviews*, *202*, 103110.

Wu, Y.-T., Higuera, P., & Liu, P. L.-F. (2021). On the evolution and runup of a train of solitary waves on a uniform beach. *Coast. Eng.*, *170, 104015*, 1–22.